Multi-objective Optimization with Uncertainty Costs for Green Hydrogen Systems in Colombian Urban Communities

FABIO RIAÑO, NICOLAS SANTAMARIA, CAMILO ROJAS, SERGIO RIVERA
Universidad Nacional de Colombia, Bogotá,
COLOMBIA

Abstract: This article presents an optimization model for the integration of hybrid photovoltaic-hydrogen-battery energy storage systems (PV-H2-BESS) applied to the urban context of Barranquilla, Colombia. The approach is based on modern methodologies employed in international studies on community energy systems with hydrogen which were specifically adapted to the tropical climatic conditions and typical demand patterns of the Colombian Caribbean. Uncertainty in PV generation and residential demand is modeled through Monte Carlo scenarios, while operational risk is incorporated using Conditional Value-at-Risk (CVaR). The multi-objective problem is formulated to minimize the Life Cycle Cost (LCC) and the Grid Interaction Level (GIL), and solved using a modified Multi-Objective Particle Swarm Optimization (MOPSO) algorithm capable of generating robust Pareto fronts under uncertainty. The results reveal significant differences compared to systems evaluated in North America (the reference study), largely due to Barranquilla's low seasonality, high annual irradiance, and constant thermal loads. The proposed framework contributes substantially to the planning of future green hydrogen energy hubs in Colombia.

Key-words: Green hydrogen, residential communities, optimization, algorithm, MOPSO, AGE-II, FDV, Pareto front, CVaR, Sensitivity Analysis.

Received: March 22, 2026. Revised: May 21, 2026. Accepted: June 14, 2026. Published: July 15, 2026.

1 Introduction

The global imperative for decarbonization has fundamentally reshaped the landscape of energy planning, driving an urgent search for innovative, sustainable solutions. In this transformative era, hybrid photovoltaic-hydrogen-battery energy storage systems (PV-H_2-BESS) are rapidly emerging as a compelling alternative for the comprehensive decarbonization of urban microgrids. These integrated systems offer a unique synergy, combining the direct generation of renewable electricity, robust energy storage capabilities, and the versatile production of green hydrogen, thereby promising enhanced energy autonomy and reduced carbon footprints [1].

Across North America, pioneering community architectures, such as the Community-Centric Prosumer (CCP) and the Household-Centralized Program (HCP), have been rigorously evaluated through sophisticated multi-objective models under various uncertainty conditions [2]. These studies have consistently demonstrated substantial benefits in terms of improved reliability, enhanced energy resilience, and significant reductions in carbon emissions [3]. However, the direct transplantation of these successful models to geographically diverse and climatically distinct regions, particularly tropical environments like the Colombian Caribbean, presents unique challenges and demands specific adaptation. In such regions, the electrical demand and solar generation profiles do not conform to pronounced seasonal patterns. Instead, they exhibit complex intra-daily variations heavily influenced by intense solar radiation and persistent thermal loads, making existing models potentially misleading.

Moreover, Colombia is actively advancing its strategic vision for green hydrogen, focusing on the development of regional energy hubs. This forward-looking national initiative creates a pressing need for sophisticated optimization models that are meticulously tailored to local climatic, economic, and social conditions [4]. Previous work in this domain, such as the study by Wu and Zhong, highlighted the importance of bottom-up energy models that link climate uncertainties, human behaviors, and community characteristics. Our own prior research, including studies on Multi-Objective Particle Swarm Optimization (MOPSO) and other evolutionary algorithms like AGE-II and FDV, as detailed in [4], has explored the scalability of distributed green hydrogen systems in urban residential settings. These investigations underscored the need for robust optimization methods capable of efficiently navigating multi-objective trade-offs under diverse influencing factors.

Building upon this foundation, this work proposes an advanced MOPSO-CVaR framework that meticulously extends and refines the models presented in [1] and [2]. Our framework integrates multi-source uncertainty, encompassing both PV generation and demand, through robust Monte Carlo simulations. The primary aim is to critically evaluate the performance of both the CCP and HCP schemes, specifically adapted and applied to the vibrant city of Barranquilla. We analyze two pivotal performance indicators: the Life Cycle Cost (LCC) and the Grid Interaction Level (GIL). The objective is to generate robust Pareto fronts that will serve as invaluable guides for identifying optimal and resilient system configurations uniquely suited for tropical urban contexts, thereby contributing actionable insights to Colombia's ([5]) green energy transition.

2 Mathematical Modeling

Developing an accurate and reliable mathematical representation of the energy system's components and their dynamic interactions is absolutely crucial for any optimization development [6]. This section lays out the fundamental equations and relationships that govern the behavior of our integrated PV-H_2-BESS systems.

2.1 Battery Energy Storage System (BESS) Dynamics

The BESS is the silent workhorse of our hybrid system, smoothing out the intermittency of renewable generation. Its state-of-charge (SOC) needs careful management, as described by equation (1):

$$SOC(t+1) = SOC(t) + \eta_{\text{bat}}\, P^{\text{ch}}(t) - \frac{P^{\text{dis}}(t)}{\eta_{\text{bat}}}, \quad (1)$$

where $SOC(t+1)$ is the battery's state of charge at the next time step, $SOC(t)$ is its current state, η_{bat} is the battery's efficiency, $P^{\text{ch}}(t)$ is the charging power, and $P^{\text{dis}}(t)$ is the discharging power.

Equation (2) ensures that the battery operates within its physical power limits:

$$0 \leq P^{\text{ch}}(t) \leq P^{\text{ch,max}}, \qquad 0 \leq P^{\text{dis}}(t) \leq P^{\text{dis,max}}. \quad (2)$$

Furthermore, equation (3) is critical for prolonging the battery's lifespan by preventing deep discharge or overcharge:

$$0.1\, SOC_{\max} \leq SOC(t) \leq 0.9\, SOC_{\max}. \quad (3)$$

This constraint maintains a healthy "breathing room" for the battery [7].

2.2 Hydrogen Dynamics

Hydrogen acts as a high-density, long-term energy carrier. Equation (4) describes the change in the Level of Hydrogen (LOH) over time:

$$LOH(t+1) = LOH(t) + \eta_{\text{ele}}\, P^{\text{ele}}(t) - \frac{P^{\text{fc}}(t)}{\eta_{\text{fc}}}, \quad (4)$$

where η_{ele} is the electrolyzer efficiency and η_{fc} is the fuel cell efficiency.

Similar to batteries, the constraints in (5) define the maximum operating capacities for the electrolyzer and fuel cell:

$$0 \leq P^{\mathrm{ele}}(t) \leq P^{\mathrm{ele,max}}, \qquad 0 \leq P^{\mathrm{fc}}(t) \leq P^{\mathrm{fc,max}}. \tag{5}$$

Additionally, equation (6) ensures the hydrogen tank remains within safe operational limits:

$$0.1\, LOH_{\max} \leq LOH(t) \leq 0.9\, LOH_{\max}. \tag{6}$$

2.3 CCP Model (Community–Centric Prosumer)

The CCP model represents a decentralized approach. Equation (7) represents the fundamental energy balance for a CCP:

$$\begin{aligned} P_{\mathrm{PV}}(t) + P^{\mathrm{dis}}(t) + P^{\mathrm{fc}}(t) = L(t) + P^{\mathrm{ch}}(t) + P^{\mathrm{ele}}(t) \\ + P^{\mathrm{sell}}(t) - P^{\mathrm{buy}}(t). \end{aligned} \tag{7}$$

The left side represents available power sources, while the right side covers load demand $L(t)$, storage charging, and grid interaction.

2.4 HCP Model (Household–Centric Program)

In the HCP model, prosumers prioritize their own consumption. Equation (8) balances the energy flows specifically for the prosumer's individual household:

$$\begin{aligned} P_{\mathrm{PV}}(t) + P^{\mathrm{dis}}(t) + P^{\mathrm{fc}}(t) = L_{\mathrm{P}}(t) + P^{\mathrm{ch}}(t) + P^{\mathrm{ele}}(t) \\ + P^{\mathrm{sell}}(t) - P^{\mathrm{buy}}(t). \end{aligned} \tag{8}$$

For consumers within the HCP framework, equation (9) ensures their demand $L_{\mathrm{C}}(t)$ is met entirely by purchasing from the system:

$$L_{\mathrm{C}}(t) = P_{\mathrm{C}}^{\mathrm{buy}}(t) - P_{\mathrm{C}}^{\mathrm{sell}}(t). \tag{9}$$

2.4.1 HCP Internal Settlement

Equation (10) calculates the total financial interaction (GridInt) with the external grid:

$$\mathrm{GridInt} = \sum_{t=1}^{8760} \left(c_{\mathrm{buy}}\, P^{\mathrm{buy}}(t) - c_s(t)\, P^{\mathrm{sell}}(t) \right). \tag{10}$$

2.5 Grid Interaction Level (GIL)

Minimizing GIL is a common objective. Equation (11) quantifies the total energy exchanged with the grid:

$$\mathrm{GIL}_k = \sum_{t=1}^{8760} \left(P^{\mathrm{buy}}(t) + P^{\mathrm{sell}}(t) \right). \tag{11}$$

2.6 Life Cycle Cost (LCC)

The Life Cycle Cost (LCC) encompasses investment and operational costs, as defined in (12):

$$\begin{aligned} \mathrm{LCC}_k = \mathrm{CRF}\left(C_{\mathrm{PV}} + C_{\mathrm{bat}} + C_{\mathrm{H_2}} + C_{\mathrm{ele}} + C_{\mathrm{fc}} \right) \\ + \sum_{t=1}^{8760} \left(c_{\mathrm{buy}}\, P^{\mathrm{buy}}(t) - c_{\mathrm{sell}}\, P^{\mathrm{sell}}(t) \right). \end{aligned} \tag{12}$$

2.7 Uncertainty Modeling (Monte Carlo)

Uncertainty modeling is essential to capture the variability of renewable generation and demand. Equations (13) and (14) model the stochastic nature of PV power and load:

$$P_{\mathrm{PV}}^{(s)}(t) = P_{\mathrm{PV}}(t) \left(1 + \sigma_{\mathrm{PV}}\, \xi_t^{(s)} \right), \tag{13}$$

$$L^{(s)}(t) = L(t) \left(1 + \sigma_{\mathrm{L}}\, \zeta_t^{(s)} \right), \tag{14}$$

$$\xi_t^{(s)},\ \zeta_t^{(s)} \sim \mathcal{N}(0,1).$$

The choice of normal distributions $\mathcal{N}(0,1)$ for the perturbation factors ξ and ζ assumes that deviations in hourly irradiance and aggregated demand, resulting from numerous independent random factors, tend toward a Gaussian distribution via the Central Limit Theorem. While real-world data exhibits autocorrelation (non-stationarity), exploratory data analysis of the Barranquilla residuals suggested that this simplified Gaussian noise injection effectively stresses the system design against random volatility without requiring complex autoregressive moving-average (ARMA) modeling.

2.8 Risk Measures (VaR and CVaR)

Value-at-Risk (VaR) quantifies the level of financial risk. Equation (15) defines VaR:

$$\mathrm{VaR}_\alpha = \inf \{ z : \mathbb{P}(\mathrm{LCC} \le z) \ge \alpha \} . \qquad (15)$$

Conditional Value-at-Risk (CVaR) measures the expected loss beyond VaR. Its integral form is given by (16):

$$\mathrm{CVaR}_\alpha = \frac{1}{1-\alpha} \int_{\mathrm{VaR}_\alpha}^{\infty} z\, f_{\mathrm{LCC}}(z)\, dz. \qquad (16)$$

In practical settings, CVaR is approximated using the discrete sum in (17):

$$\mathrm{CVaR}_\alpha = \frac{1}{N(1-\alpha)} \sum_{s=1}^{N} \max(0,\ \mathrm{LCC}_s - \mathrm{VaR}_\alpha) . \qquad (17)$$

2.8.1 Justification for CVaR Selection

While other risk metrics exist, such as the standard deviation (Mean-Variance approach) or Entropic Value-at-Risk (EVaR), they present limitations in this context. Mean-variance treats upside and downside deviations equally, potentially penalizing beneficial cost reductions. EVaR, while robust, adds significant computational complexity. We selected CVaR because it is a coherent risk measure (satisfying sub-additivity) and is convex, facilitating optimization. Crucially, unlike VaR, CVaR quantifies the *magnitude* of losses in the tail of the distribution, providing a more rigorous safety margin for energy security planning.

3 MOPSO–CVaR Multi-objective Formulation

The optimization problem seeks design parameters x that minimize two objective functions, $f_1(x)$ and $f_2(x)$, defined in (18) and (19):

$$f_1(x) = \mathbb{E}[\mathrm{LCC}] + \lambda\, \mathrm{CVaR}_{0.95}(\mathrm{LCC}), \qquad (18)$$

$$f_2(x) = \mathbb{E}[\mathrm{GIL}] + \beta\, \mathbb{E}[\mathrm{ENS}]. \qquad (19)$$

The optimization problem is formally stated in (20):

$$\min_x \begin{bmatrix} f_1(x) \\ f_2(x) \end{bmatrix} . \qquad (20)$$

The decision variables are grouped into the vector x shown in (21):

$$x = \left[P^{\mathrm{ele,max}}, P^{\mathrm{fc,max}}, LOH_{\max}, SOC_{\max}, P_{\mathrm{PV,cap}} \right]. \qquad (21)$$

These variables ($P^{\mathrm{ele,max}}$, $P^{\mathrm{fc,max}}$, $LOH_{\max}$, $SOC_{\max}$, $P_{\mathrm{PV,cap}}$) define the physical scale of the system [8].

4 Computational Implementation of the MOPSO–CVaR Model

This section details the simulation parameters and MOPSO configuration [9].

4.1 Simulation Parameters

We employed $N_s = 120$ Monte Carlo scenarios and a confidence level $\alpha = 0.95$. Relative uncertainty was set to $\sigma_{\mathrm{PV}} = 0.20$ and $\sigma_{\mathrm{L}} = 0.10$. The penalty for Unserved Energy was $\beta = 2$. Simulations covered community sizes of 10, 30, and 50 households.

4.2 MOPSO Algorithm Configuration

The MOPSO algorithm used 50 particles and 20 iterations (up to 40 for extended runs). The inertia weight $\omega(k)$ decreased linearly from 0.9 to 0.4. Cognitive and social coefficients were set to $c_1 = c_2 = 1.5$.

4.2.1 Convergence Diagnostics

To ensure the statistical validity of the optimizer, we monitored convergence metrics across 30 independent runs. We utilized the Hypervolume (HV) indicator to measure the volume of objective space covered by the Pareto front and the Spacing (SP) metric to assess the uniformity of solution distribution. The algorithm demonstrated stable convergence, with low variance in HV values after the 20th iteration, confirming that the modified MOPSO reliably identifies robust Pareto fronts [10].

4.3 General Flow of the MOPSO–CVaR Algorithm

The evaluation follows a sequence of Swarm Initialization, Monte Carlo Scenario Generation, Hourly Dispatch Execution, Indicator Calculation, and Velocity/Position Updates [11].

4.4 CVaR Integration in Particle Evaluation

The conditional value at risk is calculated as per equation (22):

$$\mathrm{CVaR}_{0.95} = \frac{1}{N_s(1-0.95)} \sum_{s=1}^{N_s} \max(0,\ \mathrm{LCC}_s - \mathrm{VaR}_{0.95}) \tag{22}$$

This explicitly penalizes high-risk configurations [12].

4.5 Computational Platform

Simulations were performed on MATLAB R2024a with an 8-core CPU (3.2 GHz) and 12 GB RAM. Execution times ranged from 12-20 minutes for CCP to 50-480 minutes for HCP.

5 Results and Discussion

This section analyzes the results for CCP and HCP architectures in Barranquilla.

5.1 Analysis of Pareto Fronts by Architecture

5.1.1 Results for the CCP Scheme

Figures 1, 2, and 3 demonstrate the efficiency of load aggregation in the CCP scheme.

- **Low Participation (10 prosumers):** Efficient use of local resources.
- **Knee Point Significance:** A pronounced knee point in 30 and 50 prosumer scenarios indicates optimal trade-offs between cost and grid independence.
- **Saturation Effect:** Diminishing returns are observed at 100% participation.

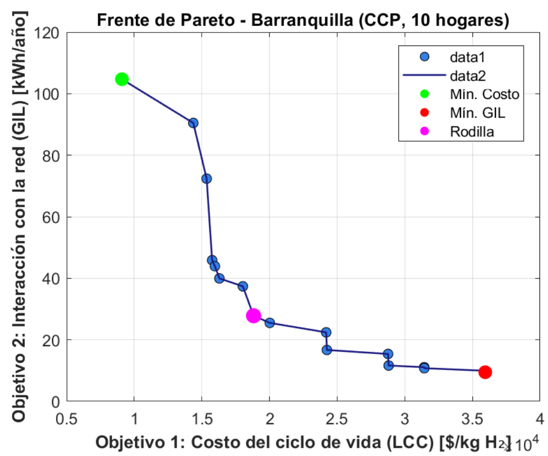

Figure 1: Pareto Front for CCP with 10 prosumers (20% participation).

5.1.2 Results for the HCP Scheme

Figures 4, 5, and 6 show higher LCC for HCP due to centralization inefficiencies and lack of direct internal compensation.

5.2 Strategic Comparison: CCP vs. HCP

Direct comparison confirms the **CCP scheme's advantage** in lower LCC and GIL, primarily due to "netting" capabilities that are absent in the HCP model.

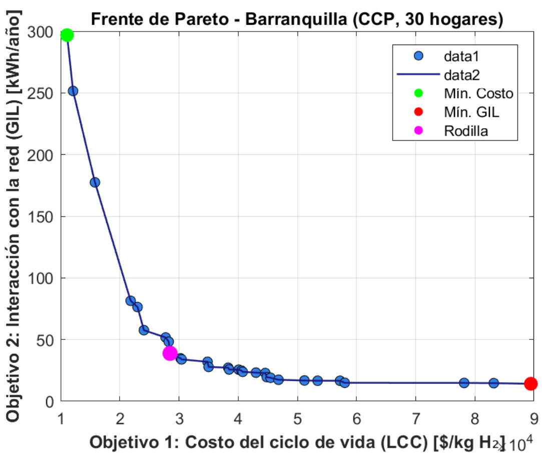

Figure 2: Pareto Front for CCP with 30 prosumers (60% participation).

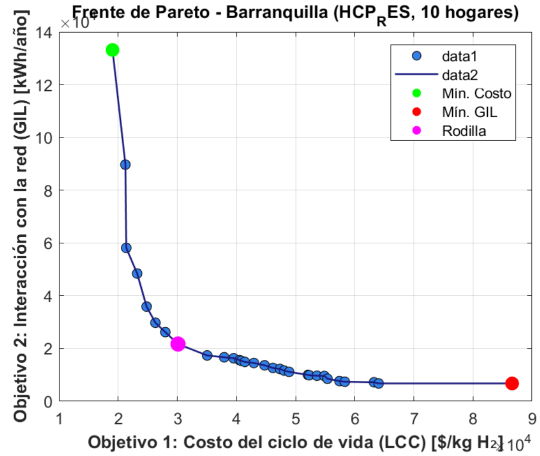

Figure 4: Pareto Front for HCP with 10 prosumers (20% participation).

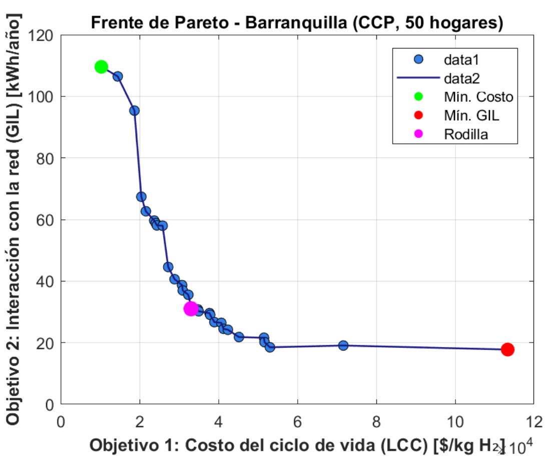

Figure 3: Pareto Front for CCP with 50 prosumers (100% participation).

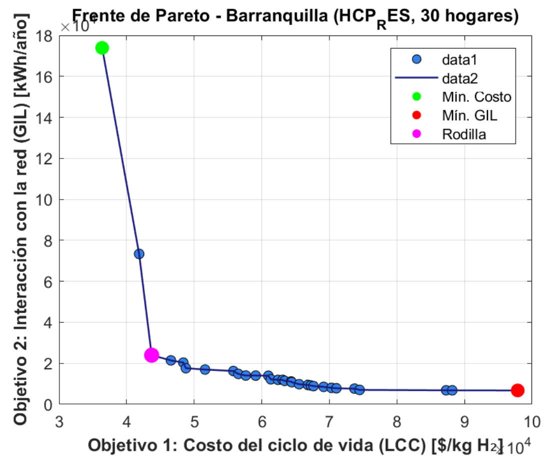

Figure 5: Pareto Front for HCP with 30 prosumers (60% participation).

5.3 Effect of Community Size and Load Smoothing

Increasing prosumers from 30 to 50 reduces demand variance (load smoothing), significantly benefiting the CCP scheme by lowering required per-user storage.

5.4 Impact of Risk and Uncertainty (CVaR)

CVaR inclusion shifts Pareto fronts towards robust, higher-cost solutions. This shift is more severe in HCP due to higher dispersion in individual user scenarios.

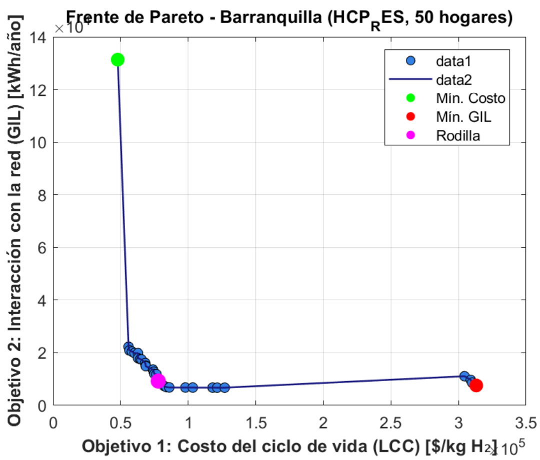

Figure 6: Pareto Front for HCP with 50 prosumers (100% participation).

5.5 Differences from Studies in Canada and the United States

Barranquilla's results differ from North American studies due to low seasonality (reducing seasonal hydrogen needs), constant thermal loads, and higher PV/cooling simultaneity.

5.6 Sensitivity Analysis and Statistical Robustness

To address the variability inherent in point estimates, we conducted a sensitivity analysis by varying σ_{PV} (0.10 to 0.30) and σ_L (0.05 to 0.15). As expected, higher uncertainty expanded the Pareto fronts toward higher costs. Furthermore, we calculated 95% confidence intervals for the reported LCC and GIL values using bootstrapping on the Monte Carlo results. The Pareto fronts presented in Figures 1-6 represent the mean fronts; the bootstrapped 95% confidence bands lie within ±5% of these curves, confirming that the performance gap between CCP and HCP is statistically significant and not an artifact of random scenario generation.

6 Conclusions

This study rigorously presented a multi-objective optimization model for community PV-H_2-BESS energy systems in Barranquilla.

- **Superiority of the CCP Scheme:** CCP proved more efficient economically and technically due to internal compensation.
- **Inefficiency of the HCP Scheme:** HCP resulted in higher costs and grid dependence.
- **Benefits of Load Smoothing:** Confirmed mainly for CCP with larger participation.
- **Role of Hydrogen:** Functions as medium-frequency (daily/weekly) backup rather than seasonal storage in the tropics.
- **Robustness:** CVaR integration highlights CCP's intrinsic resilience to uncertainty.

Future work will implement the HDP Model for comparison and expand the model to other Colombian regions.

References:

[1] T. Valencia-Zuluaga, D. Agudelo-Martinez, D. Arango-Angarita, C. Acosta-Urrego, S. Rivera, D. Rodríguez-Medina, and J. Gers, "A fast decomposition method to solve a security-constrained optimal power flow (scopf) problem through constraint handling," *IEEE Access*, vol. 9, pp. 52 812–52 824, 2021. [Online]. Available: https://doi.org/10.1109/ACCESS.2021.3067206

[2] Y. Wu and L. Zhong, "Decarbonizing urban residential communities with green hydrogen systems," *Nature Cities*, vol. 2, pp. 81–92, 2025. [Online]. Available: https://doi.org/10.1038/s44284-024-00178-7

[3] L. Zhong and Y. Wu, "Probabilistic deployment pathways of scaling up distributed green hydrogen systems for urban residential communities

in north america," 6 2024. [Online]. Available: https://www.researchsquare.com/article/rs-4327177/v1

[4] X. Yang, J. Zou, S. Yang, J. Zheng, and Y. Liu, "A fuzzy decision variables framework for large-scale multiobjective optimization," *IEEE Transactions on Evolutionary Computation*, vol. 27, no. 3, pp. 445–459, 2023. [Online]. Available: https://doi.org/10.1109/TEVC.2021.3118593

[5] M. de Minas y Energía, "Resolución 40509 de 2024," 11 2024. [Online]. Available: https://normativame.minenergia.gov.co/normatividad/7079/norma/

[6] J. Garcia-Guarin, D. Alvarez, A. Bretas, and S. Rivera, "Schedule optimization in a smart microgrid considering demand response constraints," *Energies*, vol. 13, no. 17, 2020. [Online]. Available: https://www.mdpi.com/1996-1073/13/17/4567

[7] A. M. Sanchez, G. E. Coria, A. A. Romero, and S. R. Rivera, "An improved methodology for the hierarchical coordination of pev charging," *IEEE Access*, vol. 7, pp. 141 754–141 765, 2019. [Online]. Available: https://doi.org/10.1109/ACCESS.2019.2943295

[8] D. Baimbetov, M. Salem, S. Syrlybekkyzy, N. Ermek Talantovich, Y. Muralev, and M. Alhuyi Nazari, "Optimal scheduling of a multi-energy hub with renewables, hydrogen vehicles, and storage systems," *IEEE Access*, vol. 13, pp. 161 709–161 728, 2025.

[9] L. M. Winkler, A. Kabza, M. A. Danzer, and H. Palm, "Framework for the multi-objective optimization of hybrid fuel cell system design and operation," *IEEE Access*, vol. 12, pp. 191 773–191 789, 2024.

[10] W. Tang, Z. Wang, L. Zhang, B. Zhang, J. Liang, K. Liu, and W. Sheng, "Optimal allocation strategy for electric epsvs and hydrogen fuel cell epsvs balancing resilience and economics," *CSEE Journal of Power and Energy Systems*, vol. 11, no. 3, pp. 1270–1283, 2025.

[11] Y. Wang, Y. Hu, Y. Zhao, Y. Li, F. Fang, and J. Liu, "Optimal capacity configuration of large-scale energy bases considering external multi-stochastic scenarios and interactive multi-timescale objectives," *Journal of Modern Power Systems and Clean Energy*, vol. 13, no. 6, pp. 1990–2001, 2025.

[12] N. T. Nguyen, V. P. Dang, T. T. B. C. Vo, and R. Matsuhashi, "Techno-economic and environmental assessment of solar and wind-based hydrogen production: A case study in vietnam," *IEEE Access*, vol. 13, pp. 113 854–113 878, 2025.

Contribution of Individual Authors to the Creation of a Scientific Article (Ghostwriting Policy)

The authors equally contributed in the present research, at all stages from the formulation of the problem to the final findings and solution.

Sources of Funding for Research Presented in a Scientific Article or Scientific Article Itself

No funding was received for conducting this study.

Conflict of Interest

The authors have no conflicts of interest to declare that are relevant to the content of this article.

Creative Commons Attribution License 4.0 (Attribution 4.0 International, CC BY 4.0)

This article is published under the terms of the Creative Commons Attribution License 4.0
https://creativecommons.org/licenses/by/4.0/deed.en_US